biotin labeling of the 4.3-kbp molecules and gel electrophoresis. An additional specific band (marked by a red arrow) that was absent in the control reactions is shown in Fig. 4A. By excising the additional band from the gel, extracting the DNA, and spreading it on a solid support, we verified that the specific band comprises DNA junctions. AFM images of such a junction are shown in Fig. 4C. These junctions can serve as a template for a three-terminal device.

The realization of sequence-specific molecular lithography constitutes an important step toward integrated DNA-templated electronics. Homologous recombination by RecA operates on scales varying between a few bases (nanometers) to thousands of bases (micrometers) with essentially single-base accuracy (~0.3 nm). Thus, our molecular lithography can operate on a broad range of length scales with essentially nanometer resolution. The various molecular lithography processes demonstrated above can be carried out sequentially; for example, junction definition followed by specific metallization of the unprotected junction's arms and colloid localization at the junction represent three levels of lithography. Molecular lithography can be applied to other DNA-programmed constructs (e.g., for mechanical applications). The resist function provided by the RecA protein can most likely be extended to operations other than metallization, because the protein apparently blocks the access of even small molecules (Ag ions in the present case) to the DNA substrate.

References and Notes

1. C. M. Lieber, *Sci. Am.* **285**, 58 (September 2001).
2. C. Joachim, J. K. Gimzewski, A. Aviram, *Nature* **408**, 541 (2000).
3. A. Bachtold, P. Hadley, T. Nakanishi, C. Dekker, *Science* **294**, 1317 (2001).
4. Y. Huang *et al.*, *Science* **294**, 1313 (2001).
5. C. M. Niemeyer, *Curr. Opin. Chem. Biol.* **4**, 609 (2000).
6. J. J. Storhoff, C. A. Mirkin, *Chem. Rev.* **99**, 1849 (1999).
7. E. Winfree, F. Liu, L. A. Wenzler, N. C. Seeman, *Nature* **394**, 539 (1998).
8. E. Braun, Y. Eichen, U. Sivan, G. Ben-Yoseph, *Nature* **391**, 775 (1998).
9. Y. Eichen, E. Braun, U. Sivan, G. Ben-Yoseph, *Acta Polym.* **49**, 663 (1998).
10. M. M. Cox, *Prog. Nucleic Acid Res. Mol. Biol.* **63**, 311 (2000).
11. λ-DNA (Promega, Madison, WI) was precipitated with ethanol to remove tris traces and dissolved in 25 mM Hepes buffer (pH 7.5) with 4 mM MgAc (final DNA concentration of 0.1 μg/μl). The DNA was incubated with 0.2% glutaraldehyde for 20 min at room temperature and then for 20 min on ice. Excess glutaraldehyde was filtered out by overnight dialysis. Aldehyde-derivatized DNA molecules were stretched on doped passivated silicon and then incubated in the dark with a 0.1 M solution of $AgNO_3$ (purity 99.9%, Carlo Erba Reagents, Milan, Italy) in 25% ammonia buffer (pH 10.5) (titrated with 70% HNO_3) at room temperature for a few hours. Gold metallization (*15*) was performed after gently washing off excess Ag with water.
12. Materials and methods are available as supporting online material on *Science* Online.
13. L. J. Ferrin, R. D. Camerini-Otero, *Science* **254**, 1494 (1991).
14. W. Szybalski, *Curr. Opin. Biotechnol.* **8**, 75 (1997).
15. A unit volume of KSCN (60 mg/ml) was mixed with a unit volume of $KAuCl_4$ (23 mg/ml) and centrifuged for 1 min at 4000*g*. The supernatant was removed, and the precipitate was mixed with 8 unit volumes of 1 M phosphate buffer (pH 5.5). Finally, a unit volume of hydroquinone (5.5 mg/ml) was added. The sample was instantly immersed in this solution and left to incubate for 0.5 to 3 min (*21*).
16. J. Richter *et al.*, *Adv. Mater.* **12**, 507 (2000).
17. S. M. Honigberg, R. B Jagadeeshwar, C. M. Radding, *Proc. Natl. Acad. Sci. U.S.A.* **83**, 9586 (1986).
18. T. Sato, H. Ahmed, D. Brown, B. F. G. Johnson, *J. Appl. Phys.* **82**, 696 (1997).
19. C. Mao, S. Weiqiong, N. C. Seeman, *J. Am. Chem. Soc.* **121**, 5437 (1999).
20. B. Muller, I. Burdett, S. C. West, *EMBO J.* **11**, 2685 (1992).
21. Y. Eichen, U. Sivan, E. Braun, PCT WO0025136 (international patent application) (1999) (http://ep.espacenet.com).
22. D. Bensimon, A. J. Simon, V. Croquette, A. Bensimon, *Phys. Rev. Lett.* **74**, 4754 (1995).

23. We acknowledge financial support by the European Commission 5th Framework Program project number IST-1999-1309S, the Israel Science Foundation, and the Rosenbloom Foundation. K.K. acknowledges support by the Clore Foundation.

Supporting Online Material

www.sciencemag.org/cgi/content/full/297/5578/72/DC1
Materials and Methods
Figs. S1 and S2

25 February 2002; accepted 13 May 2002

Global Distribution of Neutrons from Mars: Results from Mars Odyssey

W. C. Feldman,[1]* W. V. Boynton,[2] R. L. Tokar,[1] T. H. Prettyman,[1] O. Gasnault,[1] S. W. Squyres,[3] R. C. Elphic,[1] D. J. Lawrence,[1] S. L. Lawson,[1] S. Maurice,[4] G. W. McKinney,[1] K. R. Moore,[1] R. C. Reedy[1]

Global distributions of thermal, epithermal, and fast neutron fluxes have been mapped during late southern summer/northern winter using the Mars Odyssey Neutron Spectrometer. These fluxes are selectively sensitive to the vertical and lateral spatial distributions of H and CO_2 in the uppermost meter of the martian surface. Poleward of ±60° latitude is terrain rich in hydrogen, probably H_2O ice buried beneath tens of centimeter-thick hydrogen-poor soil. The central portion of the north polar cap is covered by a thick CO_2 layer, as is the residual south polar cap. Portions of the low to middle latitudes indicate subsurface deposits of chemically and/or physically bound H_2O and/or OH.

Neutron spectroscopy can be used to survey planetary bodies for hydrogen (*1*). The epithermal neutron energy range (0.4 to about 500 keV) is most sensitive for this purpose. Measurements of thermal (<0.4 eV) and epithermal neutron fluxes also provide unique information about the existence and thickness of deposits of CO_2 (*2*). Such deposits are expected to cover both martian polar caps during their respective winter months (*3*–*5*), and CO_2 is also thought to blanket the residual south polar cap of Mars (*5*–*7*).

A component of the Gamma-Ray Spectrometer (GRS) aboard Mars Odyssey is the Neutron Spectrometer (NS) (*8*, *9*). For the purposes of our initial global survey of neutrons produced by Galactic cosmic rays that leak away from Mars, we used data collected between 20 March and 18 April 2002, covering areocentric Sun longitudes between about 345° and 360° (late in southern summer/northern winter). An estimation of the abundance and stratigraphy of hydrogen near the south martian pole using gamma-ray and neutron data is presented separately (*10*).

The NS consists of a cubical block of boron-loaded plastic scintillator that is segmented into four individual prism-shaped sensors (*9*). During mapping, the four sensors are oriented with one facing down toward Mars, one facing in the forward direction nearly along the spacecraft's velocity vector (V_{sc}), one facing backward, nearly antiparallel to V_{sc}, and one facing upward (*11*). The difference in counting rates between the forward- and backward-facing sensors is a reliable estimate of the counting rate across the thermal energy band because the backward sensor measures the epithermal and spacecraft components. The downward-facing sen-

[1]Los Alamos National Laboratory, Los Alamos, NM 87545, USA. [2]University of Arizona, Lunar Planetary Laboratory, Tucson, AZ 85721, USA. [3]Cornell University, Center for Radiophysics and Space Research, Ithaca, NY 14853, USA. [4]Observatoire Midi-Pyrénées, 31400 Toulouse, France.

*To whom correspondence should be addressed. E-mail: wfeldman@lanl.gov

sor is covered by cadmium. The combination of its orientation relative to Mars and its position on the spacecraft provides it with optimal sensitivity to epithermal neutrons from Mars, with minimal neutron background from the spacecraft.

We used 25.7 days of mapping-orbit data in the present survey of neutrons from Mars. Maps of thermal neutrons were constructed using the difference in counting rates due to the $^{10}B(n,\alpha)^{7}Li$ reaction registered by the front- and back-facing sensors. Maps of epithermal neutrons show counts measured by the downward, cadmium-covered sensor. Maps of fast neutrons show the counts registered in the lowest channel of fast-neutron pulse-height spectra. (*9*). All four sensors were summed, yielding a measure of the combined count rate of fast neutrons coming from Mars and the spacecraft. The count rates shown in the maps are proportional to the flux of neutrons leaking from the surface.

The flux of thermal neutrons is highest north of about +80° latitude (Figs. 1 and 2, top). This flux distribution is nearly symmetric around the north pole but has a small equatorial extension that is centered at 330° east longitude. This zone of maximum thermal flux intensity is surrounded by an annulus of relative minimum intensity (blue color in the maps) that extends equatorward to about +55°, with a maximum equatorial excursion to about +45° latitude between 120° and 285° east longitudes (Figs. 1 and 2, top).

The thermal flux intensity is also low south of about –55° latitude. There is a small enhancement of thermal flux that is centered at about –87° latitude, between about 325° and 345° east longitude. The large-scale reduction in thermal flux at the south pole has a small equatorward extension to about –50° latitude centered at about 105° east longitude. An overview of the equatorial portions of the thermal maps shows only small relative variations.

The epithermal maps (Figs. 1 and 2, middle) show discrete regions of low fluxes. The south-polar region is delineated by a low flux that exists poleward of –60° latitude but extends equatorward to about –50° latitude, between about 75° and 130° east longitude. Although most of the north-polar region also has low epithermal fluxes, a relative minimum occurs near +60° latitude, between about 205° and 275° east longitude. A globally similar pattern of epithermal neutron flux is measured using the High Energy Neutron Detector (*12*).

Equatorward of ±45°, distinct regions of high and low fluxes can be seen. The highest epithermal fluxes come from just north of Argyre Basin and in Solis Planum. Regions of enhanced hydrogen abundance correspond to relative minima in the epithermal flux. They occur in: (i) a broad region southwest of Olympus Mons, extending to, and arcing southward and westward around Elysium Mons; (ii) a broad area that extends between –30° and +35° latitude and between 355° and 50° east longitude; (iii) a small region centered on +5° latitude between 310° and 330° east longitude; (iv) a region centered on –7° latitude between 270° and 292° east longitude; and (v) a small region centered at +32° latitude and 317° east longitude.

The fast neutron maps on the bottom in Figs. 1 and 2 also show flux variations. Two salient differences, as compared to the epithermal maps are: (i) the north polar region above +60° latitude has a low flux in the fast neutron maps, whereas the central portion of the northern cap shows an increase in the epithermal flux; and (ii) variations in fast neutron fluxes equatorward of ±60° latitude are lower than those for epithermal neutrons. The similarity of the fast and epithermal maps is quantified in the scatter plot of fast neutron versus epithermal counting rates shown in Fig. 3. A linear regression fits the data well; the correlation coefficient is $R = 0.84$.

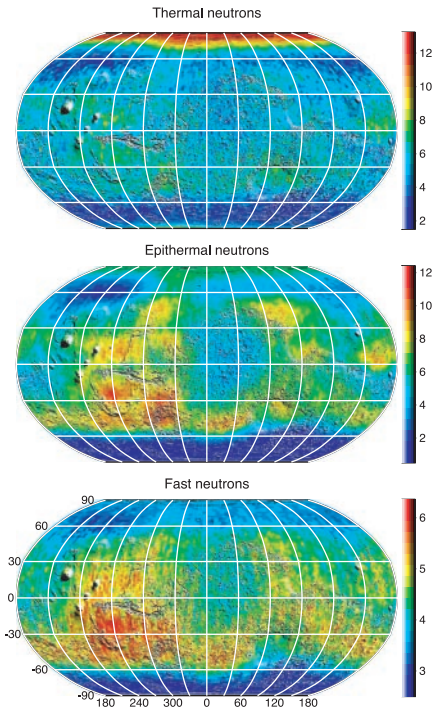

Fig. 1. Global maps of thermal (**top**), epithermal (**middle**), and fast (**bottom**) neutron counting rates. The maps are given in pseudo-cylindrical Robinson projection, and the data are binned into equal-area (1.4×10^4 km^2) spatial pixels, equivalent to about 2° × 2° at the equator. The color scales of all three maps are in units of counts s^{-1}.

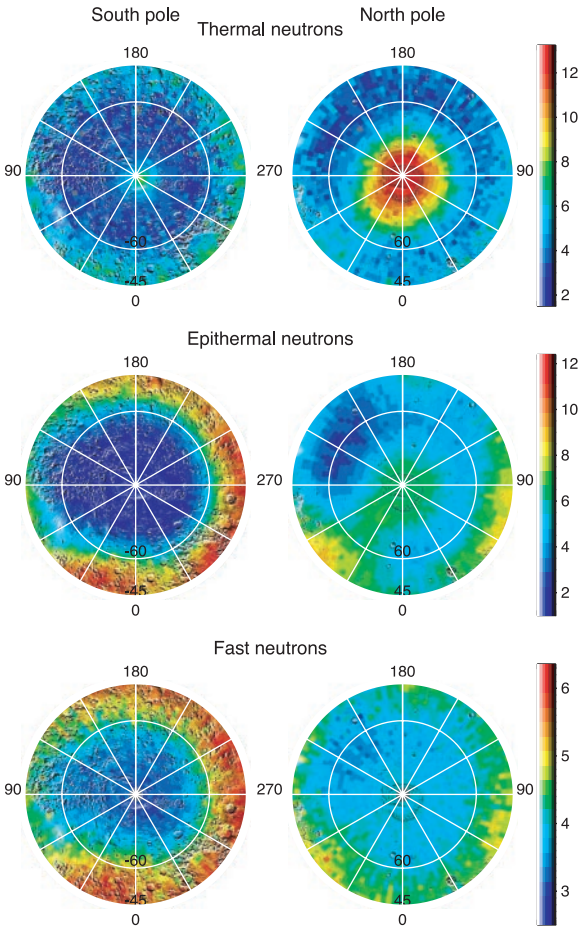

Fig. 2. Polar maps of thermal (**top**), epithermal (**middle**), and fast (**bottom**) neutron counting rates presented in stereographic projection as seen from above the south (**left column**) and north (**right column**) poles of Mars, respectively. The outermost circular contour at the north (right) and south (left) poles is at ±45° latitude, respectively.

A comparison of the range of thermal, epithermal, and fast neutron flux intensities observed at Mars (Fig. 4) shows that the flux of fast neutrons varies the least. The maximum-to-minimum fast neutron flux ratio for Mars is 2.3, which is much larger than that for the Moon, which is 1.3 (*13*). Similarly, the ranges of thermal- and epithermal-neutron fluxes from Mars span a factor of 7.2 and 9.2, respectively, whereas that of the Moon spans a factor of 3 and 1.12, respectively. (*13–15*).

The large divergence between the lunar and martian epithermal flux histograms and the strong correlation between fast and epithermal neutron fluxes have only one plausible interpretation—the surface of Mars is richer in hydrogen than that of the Moon. Both epithermal and fast flux components are reduced when hydrogen is present because of a reduction in average atomic mass of surface soils (*16*) and an increase in moderation efficiency by hydrogen (*2*, *17*). The fact that a single parameter characterizes the correlation between fast and epithermal neutrons on Mars (the slope of a linear regression) points to a single cause of the relation. In fact, a similar regression for the Moon yields a negative slope and a very poor correlation coefficient, $R = 0.32$. This conclusion is supported by the detection by the GRS of a strong 2.223-MeV gamma-ray line south of −60° latitude on Mars (*10*).

A quantitative relation between hydrogen abundance and epithermal counting rates depends on the distribution of hydrogen abundance with depth below the surface [see fig. 11 of (*2*)]. We can, in principal, sort through possible layered models by analyzing all three energy ranges of measured neutron flux intensities and the measured intensity of hydrogen neutron-capture gamma rays at 2.223 MeV (*10*). Burial of a thick hydrogen-rich soil below a thin hydrogen-poor dust layer reduces the flux of epithermal and fast neutrons, reduces the unscattered 2.223-MeV gamma-ray line intensity, and induces a double-valued trend in the flux of thermal neutrons with increasing depth of burial (*2*). As the depth of burial increases, the leakage flux of thermal neutrons first decreases, then reaches a minimum, and finally increases back to the flux that is characteristic of the thick dust soil (*2*). In contrast, the intensity of thermal neutron leakage flux from a single thick surface deposit of hydrogen increases with increasing hydrogen content before decreasing below the flux characteristic of the soil with no hydrogen.

Both martian polar regions have enhanced hydrogen content (Figs. 1 and 2). In the south, where it was summer when the data were accumulated, all three energy ranges of neutron flux begin decreasing from their equatorial plateau southward of between –50° and –55° latitude. In the north, where it was winter, all three fluxes begin to decrease northward of about +50° latitude. The neutron data at high latitudes can be explained readily by the presence of near-surface water ice. The martian regolith has been formed by impact, eolian, and other processes and may be porous and permeable. Ice can condense and persist in regolith pores if the water vapor partial pressure and the maximum annual temperature permit ice stability. If the observed martian mean atmospheric water vapor is mixed uniformly over the lower atmosphere, then subsurface pore ice that is in diffusive contact with the atmosphere will be stable on annual time scales wherever the temperature is always below about 200 K (*18*). Thermal calculations show that this condition will be met below depths of just a few tens of centimeters poleward of ±60° latitude (*18–20*), consistent with our observations. Subsurface ice at present times can also be a remnant of polar-cap glaciers that were more extensive during previous epochs.

Neither the north nor the south hydrogen epithermal fluxes are symmetric around their respective poles. The equatorial extension of the fluxes was predicted from time-dependent models of the thermal and diffusive behavior of ice in the martian regolith (*19*) and was predicted to be observable in measured leakage neutron fluxes (*2*). This agreement further supports the idea that these enhanced hydrogen deposits near both martian poles are due to subsurface water ice.

The thermal and epithermal fluxes increase as both poles are approached. Simulations (*2*) show that this rise in both fluxes is the signature of a CO_2 ice cap that covers the underlying hydrogen-rich soil. This rise cannot be due to a subsurface water-ice rich layer that approaches the surface with increasing latitude, because that would result in an increase in thermal neutrons and a decrease in epithermal neutrons, contrary to what is observed. The larger increase at the north pole, then, corresponds to seasonal CO_2 frost that precipitates out of the atmosphere to cover the polar cap during winter (*3–7*), and the smaller increase at the south corresponds to the CO_2 ice that covers the residual south-polar cap. This last association is confirmed by the offset from the actual south pole of the increase at thermal energies, coincident with the center of the south polar residual cap. The thickness of the CO_2 frost cap in the north is also not symmetric around the pole. It is greatest in both the thermal and epithermal polar maps at about 330° east longitude. This location corresponds to the topographically lowest part of the north-polar region (near Chasma Borealis), and hence the densest portion of the overlying CO_2 atmosphere. One might expect enhanced CO_2 frost precipitation under these conditions (*21*).

The neutron maps reveal variations in the concentration of hydrogen at middle to low latitudes. One prominent region of relatively high hydrogen concentration covers a large fraction of Arabia Terra and extends into Terra Meridiani and Xanthe Terra to the south and west. Another encircles both Amazonis and Elysium Planitia to the south. Relative minima in the epithermal neutron map are centered on the deepest and widest portion of Valles Marineris near the equator between 270° and 300° east longitude, and just north of +30° latitude at about 315° east longitude, at the mouth of Kasei Valles.

The concentrations of H_2O-equivalent hydrogen implied by NS observations at low to mid latitudes can be estimated by comparing thermal and epithermal counting rates measured there with those at a location on Mars

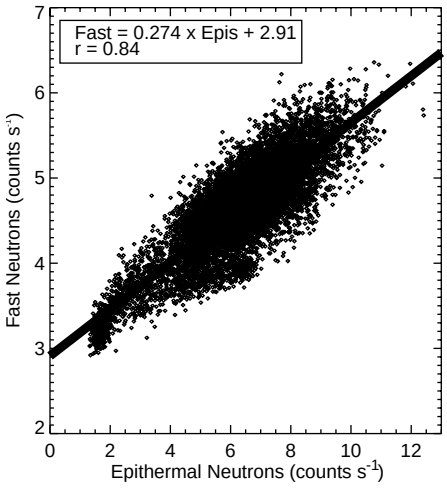

Fig. 3. Scatter plot of fast and epithermal neutrons for each equal-area pixel in Fig. 1. The straight line is the best-fitting linear regression, having a correlation coefficient of $R = 0.84$.

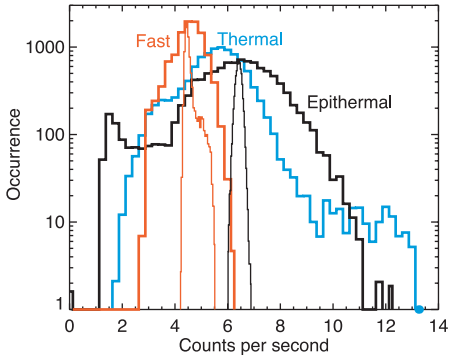

Fig. 4. Histograms of fast (red), thermal (blue), and epithermal (black) neutron counting rates. Lunar histograms of fast and epithermal neutrons have been normalized to martian counting rates and plotted over their respective martian histograms (thin lines). For ease of comparison, the lunar fast measurements were scaled to have a maximum occurrence per equal-area pixel of 2000, and those of the epithermal measurements were scaled to 650.

where we have reasonable ground-proof knowledge of the hydrogen content of surface soils. For this purpose, we chose the site of Viking 1, for which we adopt the water-equivalent hydrogen abundance from (*22*) of 1%. Our result for Arabia Terra is 3.8 ± 0.6 and 3.5 ± 0.5% at –15° latitude between 180° to 210° east longitude. If the chlorine abundance of surface soils is constant at equatorial latitudes within a factor of 3, then the measured depression in thermal neutron fluxes within these hydrogen-rich terranes implies a burial depth of about 25 to 30 g/cm^2 below hydrogen-poor soil. We therefore suspect that the variations in hydrogen concentration seen at these latitudes may primarily reflect geographic variations in the amount of chemically and/or physically bound H_2O and/or OH by minerals buried beneath a 15- to 20-cm-thick hydrogen-poor dust layer.

The near-surface martian regolith is expected to be a mix of unweathered and weathered materials. The unweathered material may be relatively coarse-grained and mostly igneous in origin, whereas weathered material may be mostly fine-grained and dominated by some mixture of palagonite and clays. The ratio of weathered to unweathered material, as well as the dominant grain size, may depend sensitively on what geologic processes have been most important in modifying the upper regolith on regional scales. For example, regions of net accumulation of windblown dust may be richer in fine-grained weathered material than are regions of net erosion.

The hydrogen content of such a regolith could be high and quite variable on regional scales. Infrared (IR) spectroscopic observations of Mars have provided clear evidence of either chemically or physically bound water in the IR-sensed surface, with concentrations of a few tenths of a percent to a few percent (*23*). The Viking GCMS experiment showed evidence for at least 1% chemically bound water in near-surface soil (*22*). Palagonite and clays can both contain substantial amounts of chemically bound water. And because fine-grained materials—clays in particular—have high specific surface areas, such materials can readily host several percent or more of adsorbed H_2O under martian near-surface conditions. So, although our data do not rule out the possibility of subsurface ice deposits at low to middle latitudes, they do not require them. We suspect instead that the NS data from these latitudes may be revealing the quantity of physically and chemically bound hydrogen in the upper tens of centimeters of martian soil that is buried beneath a 15- to 20-cm-thick layer of hydrogen-poor soil. Important sources of the observed geographic variability may include regional variations in regolith grain size and in the ratio of weathered to unweathered material over these depths.

References and Notes

1. R. E. Lingenfelter, E. H. Canfield, W. N. Hess, *J. Geophys. Res.* **66**, 2665 (1961).
2. W. C. Feldman, W. V. Boynton, B. M. Jakosky, M. T. Mellon, *J. Geophys. Res.* **98**, 20855 (1993).
3. R. B. Leighton, B. C. Murray, *Science* **153**, 136 (1966).
4. P. B. James, H. H. Kieffer, D. A. Paige, in *Mars*, H. H. Kieffer, B. M. Jakosky, C. W. Snyder, M. S. Matthews, Eds. (Univ. of Ariz. Press, Tucson, 1992), pp. 934–968.
5. P. T. Thomas, S. Squyres, K. Herkenhoff, A. Howard, B. Murray, in (*4*), pp. 767–795.
6. G. Neugebauer, G. Munch, H. H. Kieffer, S. C. Chase Jr., E. D. Miner, *Astron. J.* **76**, 719 (1971).
7. H. H. Kieffer, *J. Geophys. Res.* **84**, 8263 (1979).
8. W. V. Boynton *et al.*, *Space Science Rev.*, in preparation.
9. W. C. Feldman *et al.*, *J. Geophys. Res.*, in press.
10. W. V. Boynton *et al.*, *Science*, **297**, 81 (2002).
11. This combination of detection directionality and sensor orientation allows neutron fluxes that originate from Mars to be separated from those that come from the spacecraft. Separation at thermal energies is possible because the spacecraft travels faster than a thermal neutron ($V_{sc} \sim 3.4$ km s^{-1} and $V_{therm} \sim 1.9$ km s^{-1}), where V_{therm} is the average speed of thermal neutrons (*24*).
12. I. Mitrofanov *et al.*, *Science*, **297**, 78 (2002).
13. W. C. Feldman *et al.*, *Science* **281**, 1489 (1998).
14. W. C. Feldman *et al.*, *Science* **281**, 1496 (1998).
15. I. Genetay *et al.*, *Planet. Space Sci.*, in preparation.
16. O. Gasnault *et al.*, *Geophys. Res. Lett.* **28**, 3797 (2001).
17. W. C. Feldman *et al.*, *J. Geophys. Res.* **105**, 20347 (2000).
18. C. B. Farmer, P. E. Doms, *J. Geophys. Res.* **84**, 2881, 1979.
19. M. T. Mellon, B. M. Jakosky, *J. Geophys. Res.* **98**, 3345 (1993).
20. D. A. Paige, *Nature* **356**, 43 (1992).
21. P. B. James, B. A. Cantor, *Icarus* **154**, 131 (2001).
22. K. Biemann *et al.*, *J. Geophys. Res.* **82**, 4641 (1977).
23. L. A. Soderblom, in (*4*), pp. 557–593.
24. W. C. Feldman, D. M. Drake, *Nucl. Instr. Meth. Phys. Res.* **A245**, 182 (1986).

25. The success to date of the Neutron Spectrometer aboard Mars Odyssey owes a great debt to the large teams at Los Alamos National Laboratory, the University of Arizona, Lockheed Martin Astronautics, and Jet Propulsion Laboratory, who through their individual talents, dedication, and hard work, made it all possible. Supported in part by NASA and conducted under the auspices of the U.S. Department of Energy.

2 May 2002; accepted 21 May 2002
Published online 30 May 2002;
10.1126/science.1073541
Include this information when citing this paper.

Maps of Subsurface Hydrogen from the High Energy Neutron Detector, Mars Odyssey

I. Mitrofanov,[1] D. Anfimov,[1] A. Kozyrev,[1] M. Litvak,[1] A. Sanin,[1] V. Tret'yakov,[1] A. Krylov,[2] V. Shvetsov,[2] W. Boynton,[3] C. Shinohara,[3] D. Hamara,[3] R. S. Saunders[4]

After 55 days of mapping by the High Energy Neutron Detector onboard Mars Odyssey, we found deficits of high-energy neutrons in the southern highlands and northern lowlands of Mars. These deficits indicate that hydrogen is concentrated in the subsurface. Modeling suggests that water ice–rich layers that are tens of centimeters in thickness provide one possible fit to the data.

Some gullies on the surface of Mars have been attributed to recent water seepage and surface runoffs (*1*). To understand the hydrological processes on Mars that form surface features such as the gullies, we need to identify where water might exist. There is a small amount, column density ~10^{-3} g/cm^2, of water vapor in the atmosphere (*2*), and surface water ice is present only at the polar caps of Mars (*3–5*). Measurements of secondary neutrons produced by cosmic rays from Mars provide a direct test for hydrogen-bearing species. A deficit of high-energy neutrons at some regions on Mars may indicate the presence of water in the subsurface, because neutrons become moderated down to thermal energies in the presence of hydrogen.

Because Mars lacks a magnetic field and has a thin atmosphere, cosmic rays propagate to and interact with the surface. As a result of the cosmic ray bombardment, a large number of secondary neutrons are produced within a subsurface layer 1 to 2 m thick (*6–8*). These neutrons interact with nuclei of atoms of the subsurface material, producing emission of gamma-ray lines (*8*). Each chemical element has a unique set of these lines, so that gamma-ray spectroscopy can identify the composition of the martian subsurface.

Photons of nuclear gamma-ray lines are emitted by inelastic scattering reactions of high-energy neutrons and by capture reactions of low-energy neutrons. Therefore, the intensity of gamma-ray lines depends on the elemental compositions of the subsurface and on the spectrum and flux of neutrons. Thus, knowledge of the spectral density of neutrons is a necessary condition for determination of the elemental abundance by the method of gamma-ray spectroscopy. However, the energy spectrum of leakage neutrons also depends on the composition of subsurface material. A

[1]Institute for Space Research, Moscow 117997, Russia. [2]Joint Institute for Nuclear Research, Dubna 141980, Russia. [3]University of Arizona, Tucson, AZ 85721, USA. [4]Jet Propulsion Laboratory, Pasadena, CA 91109, USA.